

Venomancer: Towards Imperceptible and Target-on-Demand Backdoor Attacks in Federated Learning

Son Nguyen¹, Thinh Nguyen², Khoa Doan^{1,2}, and Kok-Seng Wong^{1,2}

¹ College of Engineering & Computer Science, VinUniversity, Hanoi, Vietnam

² VinUni-Illinois Smart Health Center, VinUniversity, Hanoi, Vietnam
{son.nh,thinh.nth,khoa.dd,wong.ks}@vinuni.edu.vn

Abstract. Federated Learning (FL) is a distributed machine learning approach that maintains data privacy by training on decentralized data sources. Similar to centralized machine learning, FL is also susceptible to backdoor attacks. Most backdoor attacks in FL assume a pre-defined target class and require control over a large number of clients or knowledge of benign clients' information. Furthermore, they are not imperceptible and are easily detected by human inspection due to clear artifacts left on the poison data. To overcome these challenges, we propose **Venomancer**, an effective backdoor attack that is imperceptible and allows target-on-demand. Specifically, imperceptibility is achieved by using a visual loss function to make the poison data visually indistinguishable from the original data. Target-on-demand property allows the attacker to choose arbitrary target classes via conditional adversarial training. Additionally, experiments showed that the method is robust against state-of-the-art defenses such as Norm Clipping, Weak DP, Krum, and Multi-Krum. The source code is available at <https://anonymous.4open.science/r/Venomancer-3426>.

Keywords: Backdoor attacks · Federated learning · Trustworthy AI

1 Introduction

Over the period, artificial intelligence outperformed humans in various domains, as highlighted by [1, 2, 21]. However, these achievements cannot work effectively when considering the rarity and sensitivity of real-world data, which poses challenges for sharing among servers. This motivates the emergence of federated learning (FL) as a promising solution for decentralized machine learning, enabling multiple participants to train a global model collaboratively without sharing their private data. As a result, there are extensive efforts to develop and refine FL strategies [3, 16, 35, 36], and one significant domain is backdoor attacks where adversaries can manipulate the local model updates to compromise the central server [3]. Although there are various studies have been proposed for the growth of this sub-field [10, 17, 18, 22, 28], these approaches still observe several drawbacks.

First, a noticeable problem can be seen in the poisoned data is witnessing the attack detectable [30]. The work in [34] explores the detectability of perturbations introduced in the training data, suggesting that even small changes can be identified, *posing tremendous challenges in the imperceptibility of such attack*. Next, the target backdoor class of most existing works [18, 22, 33] is pre-defined, limiting the flexibility and adaptability of the attack. Consider a scenario where a manufacturer of smart home devices employs FL to refine product performance using consumer data incrementally. In this setup, each device category corresponds to a unique class within a machine-learning model that predicts user preferences. An adversary aims to compromise the system by shifting focus across different target classes throughout the communication rounds.

In this work, we design a novel framework, named Venomancer, to overcome the aforementioned challenges (*i.e.* low imperceptibility and only pre-defined targets). We explore the arbitrary-target scenario in FL and use a visual loss to make backdoor samples resemble original images. In particular, we introduce a two-phase backdoor attack scheme, including (1) a training generator and (2) an injecting backdoor. In the first phase, the attack model can select a target class with each communication round and generate imperceptible poisoned images to fool the local model. The next phase concludes by injecting malicious clients into the global model. This mechanism effectively overcomes the previous limitations and bypasses several defenses in FL.

To evaluate our performance, we conducted thorough experiments on widely recognized benchmark datasets such as MNIST [6], Fashion-MNIST [32], CIFAR-10 [14], and CIFAR-100 [14]. Experimental results show that our method consistently achieves strong results across various datasets, particularly in the target-on-demand scenario. Moreover, we examined the robustness against four defense strategies: Norm Clipping [16], Weak DP [31], Krum [4], and Multi-Krum [4]. We then demonstrate the imperceptibility of our method.

To summarize, the main contributions of this paper are as follows:

- We introduce an effective backdoor attack scenario in FL, allowing the attacker to arbitrarily choose the target class during inference. This approach significantly increases the flexibility of the attack within the FL setting.
- We propose a new method named Venomancer that can effectively attack the global model in the above scenario by generating imperceptible backdoor samples with the utilization of a visual loss.
- Finally, we validate the efficacy and resilience of our approach against several common defense strategies through empirical evaluation. Experimental results show that our method can secure high success rates in attacks targeting any chosen class while maintaining the model’s expected performance under standard operating conditions.

Subsequently, the paper is structured as follows. In Section 2, we discuss the current attacks and defense mechanisms. The threat model is outlined in Section 3. We provide the details of the proposed methodology in Section 4 and evaluate its performance in Section 5. Section 6 provides our conclusions.

Further information regarding experimental settings and results can be found in the supplementary material.

2 Preliminaries and related works

2.1 Preliminaries

Federated Learning (FL) was initially introduced in [13] to enhance communication efficiency within decentralized learning environments. Formally, the central server initiates each communication round by randomly selecting a subset of m clients from a total pool of N clients to contribute to the training process. Every chosen client i possesses a unique local dataset, denoted as \mathcal{D}_i . At the start of the round, the server dispatches the global model’s parameters θ_{global}^{t-1} from the previous iteration to these selected clients. Each client, upon receiving these parameters, initializes its local model f_i with θ_{global}^{t-1} and proceeds to train f_i on its \mathcal{D}_i across several local epochs. This process yields updated local model weights θ_i^t , as outlined in Algorithm 1. Subsequently, each client sends the difference $(\theta_i^t - \theta_{global}^{t-1})$ back to the central server. The server then aggregates these differences from all participating clients to update the global model’s parameters to θ_{global}^t by leveraging the FedAvg algorithm [19], with the following equation:

$$\theta_{global}^t = \theta_{global}^{t-1} + \sum_{i=1}^m \frac{n_i}{n^t} (\theta_i^t - \theta_{global}^{t-1}), \quad (1)$$

where n_i is the number of samples from client i , and n^t is the total number of samples from the selected clients at round t . The FL training is repeated for a specific number of communication rounds.

2.2 Existing attacks and their limitations

The main objective of a backdoor attack in FL is to exploit vulnerabilities in local models to compromise the integrity of the global server. Since the first introduction of [3], there have been considerable efforts to construct effective backdoor attacks [10, 17, 28], and this has become one of the main threats in FL.

One notable challenge in backdoor attacks is the detectability of adversarial manipulations, especially in regions of an image with low pixel variance [15]. Early attempts to address this, such as the BFGS method [9], focused on introducing minor but impactful perturbations to legal inputs, which were still perceptible. To advance beyond visible manipulations, [22] introduced IBA, a technique that innovatively pairs a generative model for crafting invisible poisoned inputs with a mechanism for embedding a backdoor into the global model. Similarly, [18] aims to craft adversarial examples with minimal perturbation, ensuring they remain visually similar to the original inputs while still misleading automated systems. Despite this, *these backdoor samples produced by these techniques remain detectable under deep analysis or even through human eyes.*

A notable limitation of traditional backdoor attack strategies is their assumption of pre-defined target classes, which contrasts with the dynamic nature of FL. Only a limited number of studies in the literature permit adversaries to randomly select classes for attack. To the best of our knowledge, Marksman backdoor [8] is the first method that focuses on this setting, which enables the generation of an optimal trigger pattern for any chosen target class. However, *this method only applied in centralized setting*, and its applicability and effectiveness remain unexplored in the FL setting.

Due to the aforementioned drawbacks, this paper proposes a method that can operate the above properties: imperceptibility and targeting arbitrary classes.

2.3 Existing Defenses

The defensive methods in FL aim to detect and mitigate updates from malicious clients, ensuring the security of the global model. For instance, Norm Clipping [16] aims to prevent attackers from injecting malicious updates that are significantly larger in magnitude than benign updates. In contrast, Weak DP [31] introduces noise to the model or its updates to obscure the contributions of individual updates, thereby providing a level of privacy protection, and Krum [4] or Multi-Krum [4] select model updates which are closest to the others in terms of Euclidean distance, effectively ignoring outliers being malicious.

We evaluate our method through various experiments to show its effectiveness in bypassing the selected defensive mechanisms.

3 Threat Model

3.1 Attacker’s Goals

We consider the supervised learning setting where the attacker or adversary aims to inject the backdoor into the global model. The main goal of the attack is to achieve high backdoor accuracy on the backdoor task while maintaining high clean accuracy on the main task. Specifically, a trigger generator is learned during the local training of malicious clients to produce adversarial noises causing the global model to misclassify the poisoned sample. The attack ensures unaffected performance on the main task and makes the poisoned data visually imperceptible. Moreover, the adversary needs the flexibility to choose any target class during inference time and bypass defensive approaches. Therefore, we proposed our backdoor attack, as shown in Figure 1.

3.2 Attacker’s Capabilities

Following threat models in FL from previous works [3,28,29], we assume that the attacker can compromise one or more clients participating in the FL training to access their training datasets. The attacker can access the received global model’s weights and the local updates sent to the central server. Furthermore, of all the

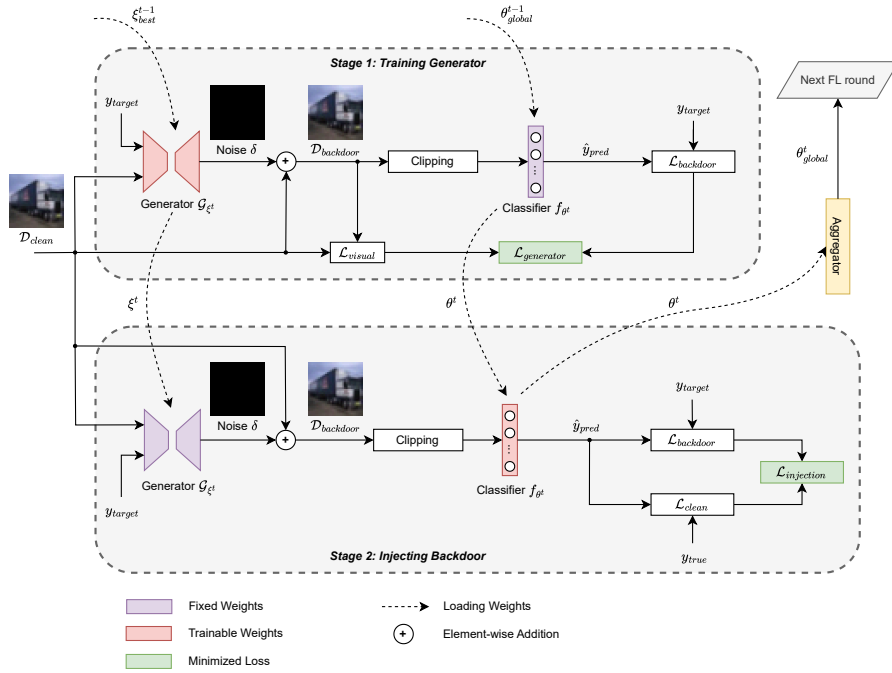


Fig. 1: Venomancer Framework. Our proposed backdoor attack consists of two training stages: (1) Training generator and (2) Injecting backdoor. Regarding the first stage, the generator G_{ξ^t} is updated using ξ_{best}^{t-1} to generate the adversarial noise δ . The generation model is trained using a combination of $\mathcal{L}_{backdoor}$, which misleads the local model into assigning poisoned images to a selected target class, and \mathcal{L}_{visual} that constrains the similarity between backdoor samples and original images. Prior to the aggregating stage after the second stage, the local model is trained to perform well on clean samples while inaccurately classifying backdoor images to the target class.

output classes of the supervised task that the attacker previously knew, he or she can choose any target classes without information about the total number of classes for the task. Moreover, the compromised clients can participate in the training for every k round, *i.e.* fixed-frequency attacks [29].

4 Proposed method

4.1 Methodology

Target-on-Demand Backdoor Attack. In the context of supervised learning, our goal is to train the classifier $f_{\theta} : \mathcal{X} \rightarrow \mathcal{Y}$ that maps an input $x \in \mathcal{X}$ to a corresponding output class $y \in \mathcal{Y}$. The classifier’s parameters θ are optimized through a training dataset $\mathcal{D} = \{(x_i, y_i)\}_{i=1}^{|\mathcal{D}|}$, where $|\mathcal{D}|$ is the total number of samples in the dataset, with $x_i \in \mathcal{X}$ and $y_i \in \mathcal{Y}$.

Algorithm 1 Local training process at round t for a benign client

Input: \mathcal{D}_{local} , θ_{global}^{t-1} , \mathcal{L} , local learning rate lr , number of local epochs E **Output:** Local model's weights θ^t **function** NormalLocalTraining $\theta^t \leftarrow \theta_{global}^{t-1}$ ▷ Initialize local model**for** epoch $e \in \{1 \dots E\}$ **for** batch $b \in \mathcal{D}_{local}$ $\theta^t \leftarrow \theta^t - lr \cdot \nabla \mathcal{L}(\theta^t, b)$ ▷ Update local model's weights**end for****end for****return** θ^t **end function**

To enhance the attacker's effectiveness, we introduce a more adaptable scenario termed "target-on-demand," which allows adversaries to choose arbitrary target classes during inference time. Particularly, this scenario can be formulated as follows:

$$f_{\theta}(x_{clean}) = y_{true}, \quad f_{\theta}(T(x_{clean}, y_{target})) = y_{target},$$

where $T(x_{clean}, y_{target})$ denotes the trigger function creating backdoor sample $x_{backdoor}$ from the clean one x_{clean} and the selected target class y_{target} , and \mathcal{Y} being the set of all possible classes in the supervised task.

Stage 1: Training Generator. Initially, the trigger generator \mathcal{G}_{ξ^t} assigned the compromised clients' aggregated parameters ξ_{best}^{t-1} , while the local model f_{θ^t} acquires the global model's weights θ_{global}^{t-1} from the prior round ($t - 1$). At this stage, the generator is trainable, but the local model's weights are fixed. Motivated by Conditional GANs [20], \mathcal{G}_{ξ^t} receives the clean dataset \mathcal{D}_{clean} and a target class y_{target} as inputs to craft adversarial noise δ . An extra embedding layer is employed within the generator to transform y_{target} into a modifiable embedding vector that signifies a trigger pattern tied to a particular target class. This adversarial noise is subsequently merged with clean samples $x_{clean} \in \mathcal{D}_{clean}$, generating the backdoor samples $x_{backdoor} \in \mathcal{D}_{backdoor}$, as shown below:

$$\delta = \mathcal{G}_{\xi^t}(x, y_{target}), \quad T_{\xi^t}(x) = x + \delta, \quad \forall x \in \mathcal{D}_{clean}.$$

Clipping is needed for $\mathcal{D}_{backdoor}$ to constrain the pixel values within the valid range. The generator is optimized to achieve two objectives: (1) $\mathcal{D}_{backdoor}$ need to be visually indistinguishable from \mathcal{D}_{clean} , and (2) $\mathcal{D}_{backdoor}$ are misclassified as y_{target} by f_{θ^t} .

Current techniques ensure the stealthiness of triggers by setting a limit, $\epsilon > 0$, on the l_{∞} norm, thus maintaining the trigger's modifications within a small, controlled range ($|\delta|_{\infty} \leq \epsilon$). However, these approaches are primarily effective in centralized settings [7, 18]. Our findings in FL reveal that this ϵ -bounded method

Algorithm 2 Local training process at round t for a malicious client

Input: \mathcal{D}_{local} , θ_{global}^{t-1} , ξ_{best}^{t-1} , \mathcal{L}_{clean} , $\mathcal{L}_{backdoor}$, y_{target} , local learning rate lr , attacker's learning rate atk_lr , number of poison epochs E_{poison} , α , β
Output: Local model's weights θ^t , attacker model's weights ξ^t

```

function BackdoorLocalTraining
     $\theta^t \leftarrow \theta_{global}^{t-1}$  ▷ Initialize local model
     $\mathcal{G}_{\xi^t} \leftarrow \xi_{best}^{t-1}$  ▷ Initialize attacker model
     $\mathcal{D}_{clean} \leftarrow \mathcal{D}_{local}$ 
    for epoch  $e \in \{1 \dots E_{poison}\}$ 
        for batch  $b_{clean} \in \mathcal{D}_{clean}$ 
            ▷ Stage 1: Training generator
             $\delta \leftarrow \mathcal{G}_{\xi^t}(b, y_{target})$  ▷ Generate adversarial noise
             $b_{poison} \leftarrow \text{Clipping}(b_{clean} + \delta)$  ▷ Create poisoned batch
             $\mathcal{L}_{generator} \leftarrow \beta \cdot \mathcal{L}_{backdoor} + (1 - \beta) \cdot \mathcal{L}_{visual}$ 
             $\xi^t \leftarrow \xi^t - atk\_lr \cdot \nabla \mathcal{L}_{generator}(\theta^t, \xi^t, b_{poison})$ 
            ▷ Stage 2: Injecting backdoor
             $\mathcal{L}_{injection} \leftarrow \alpha \cdot \mathcal{L}_{clean} + (1 - \alpha) \cdot \mathcal{L}_{backdoor}$ 
             $\theta^t \leftarrow \theta^t - lr \cdot \nabla \mathcal{L}_{injection}(\theta^t, \xi^t, b_{clean})$ 
        end for
    end for
    return  $\theta^t, \xi^t$ 
end function
    
```

falls short, leading to diminished backdoor effectiveness or poisoned data that are visually detectable. To overcome this drawback, we utilize the visual loss $\mathcal{L}_{visual}(T_{\xi}(x), x)$, for all $x \in \mathcal{D}_{clean}$, which enables the generator to identify critical regions in the original images by measuring the pixel-wise differences between clean and backdoor samples. Consequently, the attack model is refined to create perturbations enhancing the similarity between backdoor samples and their clean counterparts, ensuring a more stealthy modification. Additionally, we use cross-entropy loss $\mathcal{L}_{backdoor}(f_{\theta}(T_{\xi}(x)), y_{target})$, for all x in \mathcal{D}_{clean} and y_{target} in \mathcal{Y} , to assess the backdoor's impact. The overall generator loss, $\mathcal{L}_{generator}$, is then calculated as a combined weighted sum of \mathcal{L}_{visual} and $\mathcal{L}_{backdoor}$:

$$\mathcal{L}_{generator} = \beta \cdot \mathcal{L}_{backdoor} + (1 - \beta) \cdot \mathcal{L}_{visual} \quad (2)$$

The attacker needs to minimize $\mathcal{L}_{generator}$ to achieve aforementioned two objectives. Finally, the generator is updated using gradient descent:

$$\xi^t \leftarrow \xi^t - atk_lr \cdot \nabla \mathcal{L}_{generator}(\theta^t, \xi^t, \mathcal{D}_{backdoor}) \quad (3)$$

How to select the best generator? Given a number of compromised clients, the attacker selects the best generator $\mathcal{G}_{\xi_{best}}$ that achieves the highest local backdoor accuracy among all the compromised clients at the end of each round. The weights ξ_{best} are then used to initialize the generator of each malicious client in the next round. We observed that this approach stabilizes the training process and makes the backdoor task converge faster.

Stage 2: Injecting Backdoor. After updating the generator in the first stage, the attacker aims to inject the backdoor into the local model of the malicious client. At this phase, the weights of the generator are fixed and the local model’s weights are learnable. Adversaries’ objective is to make the local model perform normally on the clean samples \mathcal{D}_{clean} while misclassifying the backdoored data $\mathcal{D}_{backdoor}$ as the target class y_{target} . The overall loss $\mathcal{L}_{injection}$ is a combination of the clean loss $\mathcal{L}_{clean}(f_{\theta}(x), y), \forall (x, y) \in \mathcal{D}_{clean}$ (e.g. cross-entropy loss) and the backdoor loss $\mathcal{L}_{backdoor}$:

$$\mathcal{L}_{injection} = \alpha \cdot \mathcal{L}_{clean} + (1 - \alpha) \cdot \mathcal{L}_{backdoor} \quad (4)$$

This multi-objective task is formulated as follows:

$$\theta^* = \underset{\theta}{\operatorname{argmin}} \mathbb{E}_{(x,y) \sim \mathcal{D}_{clean}} \mathcal{L}_{injection}(f_{\theta}(x), y, f_{\theta}(T_{\xi}(x)), y_{target}) \quad (5)$$

After finishing the training process, the local model has learned both the clean task and the backdoor task, hence it is poisoned. Next, the client sends its malicious local updates back to the central server for aggregation. Finally, the global model is manipulated to misclassify the poisoned data as the target class y_{target} . Following the previous work [22], we choose α as 0.5 to balance the two objectives. The details for the whole training process of a malicious client are displayed in Algorithm 2.

5 Experiments

5.1 Experimental Setup

We conduct our FL experiments using the PyTorch 2.0.0 framework [23]. All experiments are done on a single machine with 252GB RAM, 64 Intel Xeon Gold 6242 CPUs @ 2.80GHz, and 6 NVIDIA RTX A5000 GPUs with 24GB RAM each. The utilized OS is Ubuntu 20.04.6 LTS.

Dataset. We evaluate our method on 4 benchmark datasets: MNIST, F-MNIST, CIFAR-10, and CIFAR-100. MNIST dataset comprises 60,000 training images and 10,000 testing images of handwritten digits, each is a 28×28 grayscale image, categorized into 10 classes. The grayscale Fashion MNIST dataset consists of 60,000 training images and 10,000 testing images of fashion items, also sized at 28×28 pixels and distributed across 10 classes. CIFAR-10 contains 50,000 training images and 10,000 testing images across 10 classes, each is a color image of size 32×32 . CIFAR-100 is similar to CIFAR-10 but has 100 classes.

Federated Learning Setup. By default, we set the number of clients $N = 100$. At the beginning of each communication round, the server randomly selects $M = 10$ clients to participate in the FL training. The global model architecture is ResNet-18 [11]. We simulate a non-i.i.d data distribution with a concentration

parameter of 0.5 by following previous works [22, 36]. Each selected client trains the local model for 2 epochs using SGD optimizer [25] with a learning rate of 0.01. The FL training period lasts for 900 communication rounds. We train the MNIST, F-MNIST, and CIFAR-10 from scratch. For the CIFAR-100 task, we use a ResNet-18 pre-trained for 60 epochs. The details of the setup are listed in the Supplementary Material.

Method Setup. The attacker compromises P out of M selected clients and is able to poison their training datasets. P malicious clients are allowed to attack in a fixed frequency of k rounds. By default, we choose $k = 1$ and $P = 2$. Following previous works [33, 36], the malicious clients are fixed during the FL training. Each malicious client has a generator that is trained in 5 epochs using Adam optimizer [12]. The weight β between the visual loss and backdoor loss is 0.01. In this work, we use an auto-encoder architecture for MNIST, F-MNIST, and CIFAR-10 and an U-Net architecture for CIFAR-100. The baseline setting for target-on-demand BadNets [10] and the details of the setup are listed in the Supplementary Material.

Evaluation Metrics.

- **Clean Accuracy (CA):** We define clean accuracy as the percentage of clean samples (samples without a trigger) that are correctly classified by the global model on the test set.
- **Backdoor Accuracy (BA):** We define backdoor accuracy as the percentage of poisoned samples that are misclassified as the target class by the global model on the test set. The higher the backdoor accuracy, the more effective the backdoor attack.

5.2 Experimental Results

This section highlights the effectiveness, robustness, and imperceptibility of our method, Venomancer. We conduct our experiments on selective benchmark datasets in a simulated FL environment. Our results demonstrate that Venomancer can achieve high BAs, high CAs, and remain undetectable by human inspection.

Table 1: Venomancer’s effectiveness across the selected datasets. The accuracies are sampled at round 900th of the FL training.

Dataset	MNIST	F-MNIST	CIFAR-10	CIFAR-100
CA (%)	99.41	90.97	69.93	58.56
BA (%)	99.52	86.28	99.66	99.46

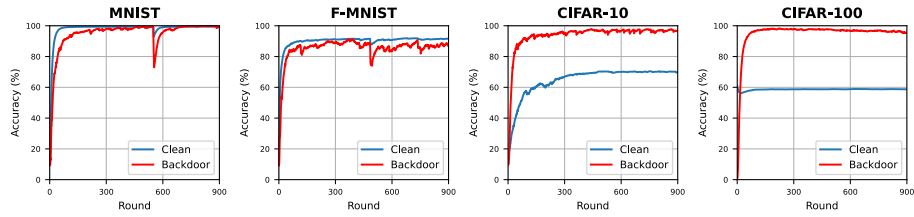


Fig. 2: Effectiveness of our method over the FL training process in selected datasets

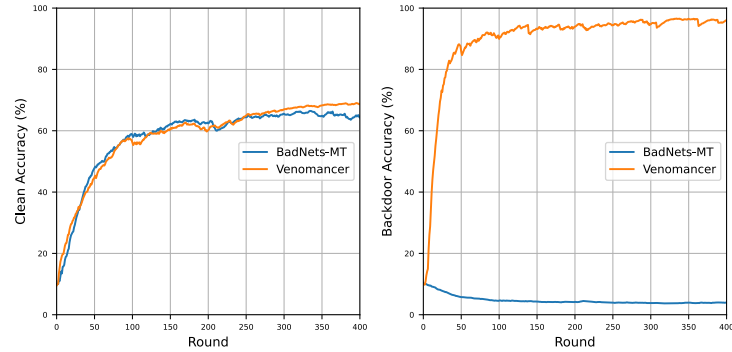


Fig. 3: An arbitrary multi-target version of the famous BadNets attack called BadNets-MT is not effective compared to our method on CIFAR-10

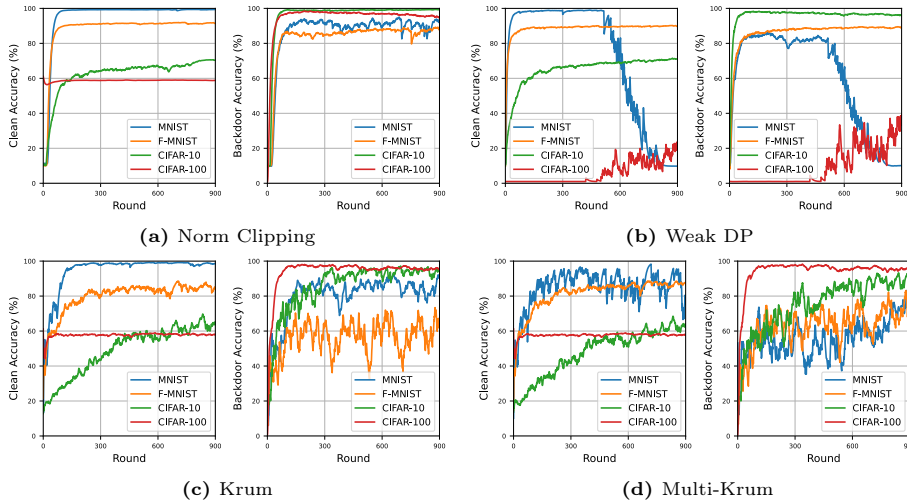
Attack performance Table 1 outlines CA and BA of our method and the baseline models under the scenario where 2% of clients are maliciously manipulated. Upon analyzing these tables, it is evident that our method consistently achieves high CA performance, exceeding 90% in MNIST and F-MNIST, and demonstrating lower rates around 70% in CIFAR-10 and 59% CIFAR-100. Despite the increased complexity of the classification task, such as the presence of 100 labels in CIFAR-100, our attack success rates remain notably superior, surpassing 88% across all datasets.

We further show that the performance of our approach is consistent across different datasets. Specifically, Figure 3 shows the CA and BA over the training process. We can observe that, the BA of our method is consistently high, exceeding 80% in the first 200 rounds.

Robustness against the selected defenses. We assess Venomancer’s effectiveness against popular defensive measures, as depicted in Figure 4. Notably, our approach demonstrates the ability to bypass Norm Clipping, Weak DP, Krum, and Multi-Krum, achieving significant backdoor accuracy (*e.g.* 94.45%, 65.79%, 96.72%, and 91.43% for the CIFAR-100 dataset, respectively). Despite fluctuations resulting from the application of defensive mechanisms, its backdoor performance consistently improves over the training process. Further results are

Table 2: Robustness of Venomancer under the selective defenses at the round 900th

Dataset	Norm Clipping		Weak DP		Krum		Multi-Krum		No-defense	
	CA (%)	BA (%)	CA (%)	BA (%)	CA (%)	BA (%)	CA (%)	BA (%)	CA (%)	BA (%)
MNIST	99.45	88.83	9.80	10.08	98.06	99.88	24.41	99.92	99.41	99.52
F-MNIST	91.41	88.09	89.98	90.68	87.51	98.00	88.36	99.44	90.97	86.28
CIFAR-10	70.62	99.13	71.44	94.91	70.16	95.19	70.42	83.20	69.93	99.66
CIFAR-100	58.93	94.45	37.90	65.79	57.97	96.72	57.60	91.43	58.56	99.46

**Fig. 4:** Our method shows the robustness against the selected defenses during the FL training period. The attack remains high BAs and CAs against considered defenses. When the BA decreases, the CA is also very low.

provided in Table 2, highlighting the method’s adeptness at evading detection strategies. Particularly, our method effectively circumvents selected defenses and maintains noteworthy backdoor accuracy. While Weak DP leads to performance decreases for specific datasets (*e.g.* MNIST by 11% and CIFAR-100 by 13%), and Krum causes declines in F-MNIST by 12% and CIFAR-10 by 18%, our method experiences minimal declines in other cases (mostly under 5%).

Imperceptible backdoor samples from our approach. In addition to being stealthy to backdoor defenses, Venomancer is expected to maintain visual imperceptibility. We assess the behavior of the attack model against Grad-CAM [26]. Figure 5 shows that the visualization heatmaps in our method are nearly identical across the clean and backdoor images. Since our method operates through input perturbation, the resulting image is formed by adding minimal perturbation to the clean image. Consequently, the differences in the latent space where the heatmaps are generated are also minimal.

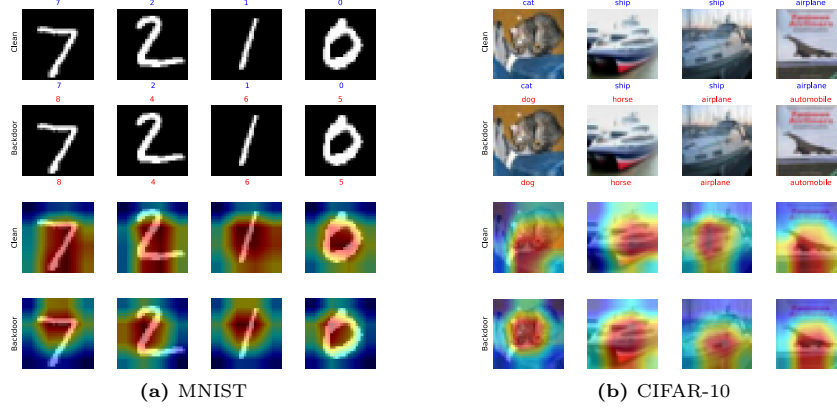


Fig. 5: Performance of our method under Grad-CAM heat maps with MNIST and CIFAR-10 datasets. The first two rows in (a) and (b) represent the clean and backdoor images in order. The last two rows represent the heat maps of the corresponding clean and backdoor images.

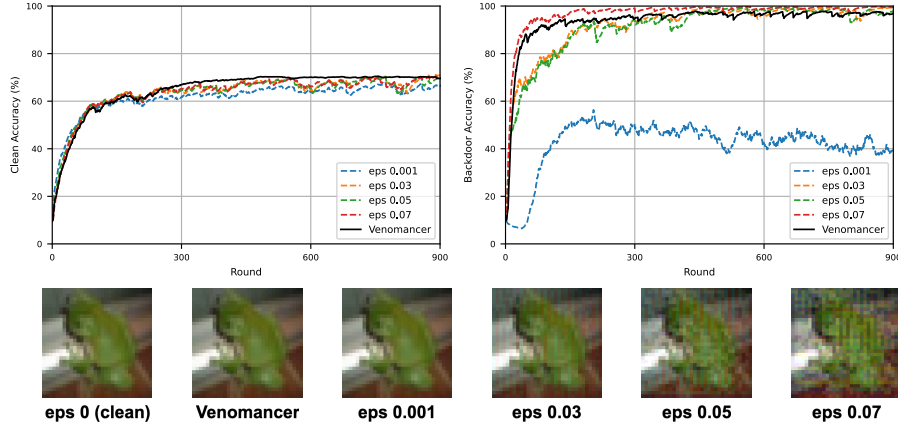


Fig. 6: Compared with our method, the popular approach of using an upper bound ϵ on l_∞ of adversarial noise shows a trade-off between BA and imperceptibility.

Effectiveness of the visual loss To be comparable with our method, a popular approach of using an upper bound ϵ on the l_∞ norm of the adversarial noise to ensure a small perturbation results in clear artifacts on the original image. Figure 6 shows that with $\epsilon = 0.07$ the BA of the l_∞ constraint approach reaches above but close to the BA of our method during the FL training but the corresponding backdoor image is not visually imperceptible, while the counterpart from our method displays an indistinguishable image from the original one. In order to get the same level of imperceptibility as Venomancer, we can choose $\epsilon = 0.001$ but the BA for this case is only around 40-50% during the whole FL training.

5.3 Limitations

Even though our method shows significant results in terms of imperceptibility and target-on-demand backdoor attacks in FL, it requires the attacker to control a certain number of participated clients to achieve high BA. Moreover, the attacker needs to poison a large number of samples in the training dataset of each malicious client to generate an effective trigger pattern. This may not be feasible in practice, especially when the number of training samples is limited. In the future, we plan to address these limitations by exploring more efficient methods to generate a good trigger with a small number of poisoned samples.

6 Conclusion

In this work, we introduce Venomancer, a backdoor attack method in FL setting, enabling adversaries to flexibly choose any target class during attacks. This method leverages a generation model alongside a visual loss to produce imperceptible backdoor samples, effectively bypassing selected defenses while maintaining the original model’s performance for benign inputs in the target-on-demand scenario. Our evaluations across datasets show our method’s effectiveness to manipulate model predictions imperceptibly. The advent of Venomancer highlights the urgent requirement for improved defenses against adaptable backdoor attacks, prompting the cyber-security field to create stronger protection methods.

References

1. Alom, M.Z., Taha, T.M., Yakopcic, C., Westberg, S., Sidike, P., Nasrin, M.S., Van Esesn, B.C., Awwal, A.A.S., Asari, V.K.: The history began from alexnet: A comprehensive survey on deep learning approaches. arXiv preprint arXiv:1803.01164 (2018) [1](#)
2. Badia, A.P., Piot, B., Kapturowski, S., Sprechmann, P., Vitvitskyi, A., Guo, Z.D., Blundell, C.: Agent57: Outperforming the atari human benchmark. In: International conference on machine learning. pp. 507–517. PMLR (2020) [1](#)
3. Bagdasaryan, E., Veit, A., Hua, Y., Estrin, D., Shmatikov, V.: How to backdoor federated learning. In: International conference on artificial intelligence and statistics. pp. 2938–2948. PMLR (2020) [1](#), [3](#), [4](#), [17](#)

4. Blanchard, P., El Mhamdi, E.M., Guerraoui, R., Stainer, J.: Machine learning with adversaries: Byzantine tolerant gradient descent. *Advances in neural information processing systems* **30** (2017) [2](#), [4](#), [20](#)
5. Chen, X., Liu, C., Li, B., Lu, K., Song, D.: Targeted backdoor attacks on deep learning systems using data poisoning. *arXiv preprint arXiv:1712.05526* (2017) [18](#), [19](#)
6. Deng, L.: The mnist database of handwritten digit images for machine learning research [best of the web]. *IEEE signal processing magazine* **29**(6), 141–142 (2012) [2](#), [16](#)
7. Doan, K., Lao, Y., Zhao, W., Li, P.: Lira: Learnable, imperceptible and robust backdoor attacks. In: *Proceedings of the IEEE/CVF international conference on computer vision*. pp. 11966–11976 (2021) [6](#), [19](#)
8. Doan, K.D., Lao, Y., Li, P.: Marksman backdoor: Backdoor attacks with arbitrary target class. *Advances in Neural Information Processing Systems* **35**, 38260–38273 (2022) [4](#)
9. Goodfellow, I.J., Shlens, J., Szegedy, C.: Explaining and harnessing adversarial examples. *arXiv preprint arXiv:1412.6572* (2014) [3](#)
10. Gu, T., Liu, K., Dolan-Gavitt, B., Garg, S.: Badnets: Evaluating backdooring attacks on deep neural networks. *IEEE Access* **7**, 47230–47244 (2019) [1](#), [3](#), [9](#), [18](#)
11. He, K., Zhang, X., Ren, S., Sun, J.: Deep residual learning for image recognition. In: *Proceedings of the IEEE conference on computer vision and pattern recognition*. pp. 770–778 (2016) [8](#), [16](#)
12. Kingma, D.P., Ba, J.: Adam: A method for stochastic optimization. *arXiv preprint arXiv:1412.6980* (2014) [9](#), [17](#)
13. Konečný, J., McMahan, H.B., Yu, F.X., Richtárik, P., Suresh, A.T., Bacon, D.: Federated learning: Strategies for improving communication efficiency. *arXiv preprint arXiv:1610.05492* (2016) [3](#)
14. Krizhevsky, A.: Learning multiple layers of features from tiny images. *Technical Report* (2009) [2](#), [16](#)
15. Liu, A., Lin, W., Paul, M., Deng, C., Zhang, F.: Just noticeable difference for images with decomposition model for separating edge and textured regions. *IEEE Transactions on Circuits and Systems for Video Technology* **20**(11), 1648–1652 (2010) [3](#)
16. Liu, J., Peng, C., Tan, W., Shi, C.: Federated learning backdoor attack based on frequency domain injection. *Entropy* **26**(2), 164 (2024) [1](#), [2](#), [4](#)
17. Liu, Y., Zou, T., Kang, Y., Liu, W., He, Y., Yi, Z., Yang, Q.: Batch label inference and replacement attacks in black-boxed vertical federated learning. *arXiv preprint arXiv:2112.05409* (2021) [1](#), [3](#)
18. Luo, B., Liu, Y., Wei, L., Xu, Q.: Towards imperceptible and robust adversarial example attacks against neural networks. In: *Proceedings of the AAAI Conference on Artificial Intelligence* (2018) [1](#), [2](#), [3](#), [6](#)
19. McMahan, B., Moore, E., Ramage, D., Hampson, S., y Arcas, B.A.: Communication-efficient learning of deep networks from decentralized data. In: *Artificial intelligence and statistics*. pp. 1273–1282. PMLR (2017) [3](#), [17](#)
20. Mirza, M., Osindero, S.: Conditional generative adversarial nets. *arXiv preprint arXiv:1411.1784* (2014) [6](#)
21. Mnih, V., Kavukcuoglu, K., Silver, D., Rusu, A.A., Veness, J., Bellemare, M.G., Graves, A., Riedmiller, M., Fidjeland, A.K., Ostrovski, G., et al.: Human-level control through deep reinforcement learning. *nature* **518**(7540), 529–533 (2015) [1](#)

22. Nguyen, T.D., Nguyen, T.A., Tran, A., Doan, K.D., Wong, K.S.: Iba: Towards irreversible backdoor attacks in federated learning. *Advances in Neural Information Processing Systems* **36** (2024) [1](#), [2](#), [3](#), [8](#), [9](#), [17](#), [19](#)
23. Paszke, A., Gross, S., Chintala, S., Chanan, G., Yang, E., DeVito, Z., Lin, Z., Desmaison, A., Antiga, L., Lerer, A.: Automatic differentiation in pytorch. In: *NIPS 2017 Workshop on Autodiff* (2017), <https://openreview.net/forum?id=BJJsrmfCZ> [8](#), [16](#)
24. Ronneberger, O., Fischer, P., Brox, T.: U-net: Convolutional networks for biomedical image segmentation. In: *Medical Image Computing and Computer-Assisted Intervention—MICCAI 2015: 18th International Conference, Munich, Germany, October 5–9, 2015, Proceedings, Part III* 18. pp. 234–241. Springer (2015) [17](#)
25. Ruder, S.: An overview of gradient descent optimization algorithms. *arXiv preprint arXiv:1609.04747* (2016) [9](#), [16](#)
26. Selvaraju, R.R., Cogswell, M., Das, A., Vedantam, R., Parikh, D., Batra, D.: Grad-cam: Visual explanations from deep networks via gradient-based localization. In: *Proceedings of the IEEE international conference on computer vision*. pp. 618–626 (2017) [11](#), [23](#)
27. Simonyan, K., Zisserman, A.: Very deep convolutional networks for large-scale image recognition. *arXiv preprint arXiv:1409.1556* (2014) [22](#)
28. Sun, Z., Kairouz, P., Suresh, A.T., McMahan, H.B.: Can you really backdoor federated learning? *arXiv preprint arXiv:1911.07963* (2019) [1](#), [3](#), [4](#), [20](#)
29. Wang, H., Sreenivasan, K., Rajput, S., Vishwakarma, H., Agarwal, S., Sohn, J.y., Lee, K., Papailiopoulos, D.: Attack of the tails: Yes, you really can backdoor federated learning. *Advances in Neural Information Processing Systems* **33**, 16070–16084 (2020) [4](#), [5](#), [17](#)
30. Wang, R., Zhang, G., Liu, S., Chen, P.Y., Xiong, J., Wang, M.: Practical detection of trojan neural networks: Data-limited and data-free cases. In: *Computer Vision—ECCV 2020: 16th European Conference, Glasgow, UK, August 23–28, 2020, Proceedings, Part XXIII* 16. pp. 222–238. Springer (2020) [2](#)
31. Wei, K., Li, J., Ding, M., Ma, C., Yang, H.H., Farokhi, F., Jin, S., Quek, T.Q., Poor, H.V.: Federated learning with differential privacy: Algorithms and performance analysis. *IEEE Transactions on Information Forensics and Security* **15**, 3454–3469 (2020) [2](#), [4](#)
32. Xiao, H., Rasul, K., Vollgraf, R.: Fashion-mnist: a novel image dataset for benchmarking machine learning algorithms. *arXiv preprint arXiv:1708.07747* (2017) [2](#), [16](#)
33. Xie, C., Huang, K., Chen, P.Y., Li, B.: Dba: Distributed backdoor attacks against federated learning. In: *International conference on learning representations* (2019) [2](#), [9](#), [17](#)
34. Yang, W., Lin, Y., Li, P., Zhou, J., Sun, X.: Rap: Robustness-aware perturbations for defending against backdoor attacks on nlp models. *arXiv preprint arXiv:2110.07831* (2021) [2](#)
35. Zhang, H., Jia, J., Chen, J., Lin, L., Wu, D.: A3fl: Adversarially adaptive backdoor attacks to federated learning. *Advances in Neural Information Processing Systems* **36** (2024) [1](#)
36. Zhang, Z., Panda, A., Song, L., Yang, Y., Mahoney, M., Mittal, P., Kannan, R., Gonzalez, J.: Neurotoxin: Durable backdoors in federated learning. In: *International Conference on Machine Learning*. pp. 26429–26446. PMLR (2022) [1](#), [9](#)

This document provides additional details, analysis, and experimental results. We begin by discussing the detailed experimental setup and implementation of our method in Appendix A. Then, we provide additional empirical experiments in Appendix B. Finally, we discuss the societal impact of our work in Appendix C.

A Training Details and Experimental Settings

A.1 Datasets

In our experiments, we use four benchmark image classification datasets, including MNIST [6], Fashion MNIST [32] (F-MNIST), CIFAR-10 [14], and CIFAR-100 [14] to evaluate our method. Those are widely used datasets in the context of backdoor attacks in FL. The usage of a dataset with more classes, *i.e.* CIFAR-100, enables better evaluation of the scalability of our target-on-demand and imperceptible backdoor attack in Federated Learning (FL). The dataset descriptions and used parameters are summarized in Table 3.

- **MNIST** is a dataset of 60,000 training images and 10,000 test images of handwritten digits (0-9), each is a 28×28 grayscale image.
- **F-MNIST** contains 60,000 training images and 10,000 test images of 10 fashion objects, also sized at 28×28 pixels.
- **CIFAR-10** consists of 50,000 training images and 10,000 test images across 10 classes, each is a color image of size 32×32 .
- **CIFAR-100** consists of 50,000 training images and 10,000 test images across 100 classes, each is a color image of size 32×32 .

We conduct our FL experiments using the PyTorch 2.0.0 framework [23]. All experiments are done on a single machine with 252GB RAM, 64 Intel Xeon Gold 6242 CPUs @ 2.80GHz, and 6 NVIDIA RTX A5000 GPUs with 24GB RAM each. The utilized OS is Ubuntu 20.04.6 LTS.

Table 3: Dataset descriptions and FL parameters

	MNIST	F-MNIST	CIFAR-10	CIFAR-100
Classes	10	10	10	100
Image Size	$28 \times 28 \times 1$	$28 \times 28 \times 1$	$32 \times 32 \times 3$	$32 \times 32 \times 3$
Total Clients	100	100	100	100
Clients/Round	10	10	10	10
Model	ResNet-18 [11]	ResNet-18	ResNet-18	ResNet-18 (*)
Optimizer	SGD [25]	SGD	SGD	SGD

(*) indicates that the model is pre-trained

A.2 Experimental Setup

We follow the FL simulation in [3, 29, 33], where the central server randomly selects a subset of clients and broadcasts its global model to every local model from participated clients. The selected clients conduct local training on their training dataset for E epochs and then send model updates back to the central server for aggregation, *i.e.* FedAvg [19]. Inspired by [3, 22, 33], we choose the number of total clients, number of participated clients per FL round, and local epochs E as summarized in Table 4.

Table 4: Task specifications and learning parameters

Task	Features	lr/E	atk_lr/E_{poison}	Batch size / Test batch size	Generator / Attacker’s optimizer
MNIST	784	0.01/2	0.0002/5	64/512	Conditional Autoencoder / Adam [12]
F-MNIST	784	0.01/2	0.0002/5	64/512	Conditional Autoencoder / Adam
CIFAR-10	3072	0.01/2	0.0002/5	64/512	Conditional Autoencoder / Adam
CIFAR-100	3072	0.001/2	0.0002/5	64/512	Conditional U-Net [24] / Adam

Following [29, 33], we simulate the heterogeneous data partition by sampling $p_k \sim Dir_K(\varphi)$. Under this strategy, non-i.i.d degree $\varphi = 0$ means the data is completely distributed (homogeneity). If $\varphi = 1$, the data distribution is absolutely non-i.i.d. To be consistent with prior works [29, 33], we select $\varphi = 0.5$ in all experiments.

Classification model. For MNIST and F-MNIST, we add one convolution layer to the original ResNet-18 architecture to convert grayscale images of $28 \times 28 \times 1$ to images of $32 \times 32 \times 3$. For CIFAR-10, we use the default ResNet-18 architecture. For CIFAR-100, the ResNet-18 model is pre-trained for 60 epochs because the model learns backdoor features quickly when it is close to vanilla convergence [3, 33] so the test accuracy for this task starts from 60.94% at the first round of the FL training. For MNIST, F-MNIST, and CIFAR-10, we train the local models from scratch. In ResNet-18, each Basic Block consists of two convolution layers, and the number of channels is doubled every time the spatial size is halved. The detailed architecture for each classifier is shown in Figure 7.

Generator model. In our experiments, we use a simple Conditional Autoencoder and a Conditional U-Net as the generator model. The Conditional Autoencoder is used for MNIST, F-MNIST, and CIFAR-10 while the Conditional U-Net is used for CIFAR-100. For Conditional U-Net, there is a component called *double_conv* which consists of two convolution layers. The input of the generator is an image and a learnable embedding vector of a target class. The detailed generator architectures are displayed in Figure 8.

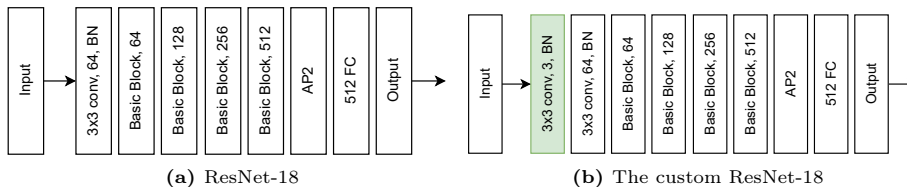


Fig. 7: The ResNet architectures used in our experiments. Green means an additional layer.

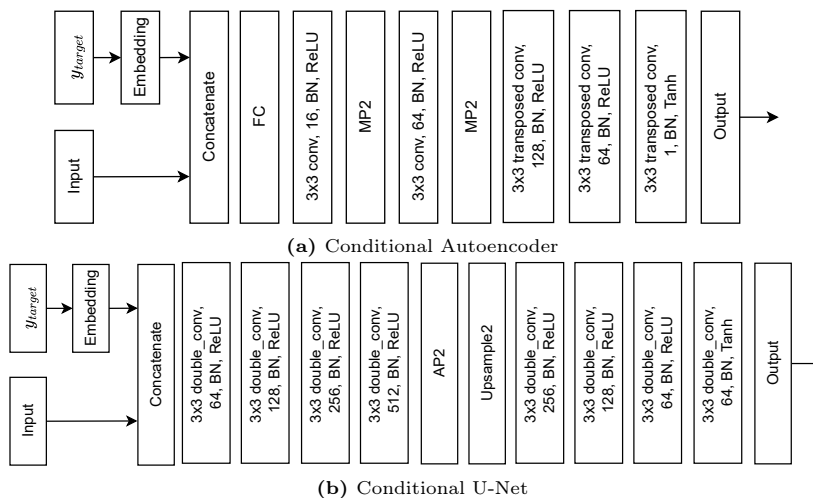


Fig. 8: The generator architectures are used in our experiments. The size of a target class embedding vector equals to the number of possible labels, *i.e.* 10 for MNIST, F-MNIST, and CIFAR-10, and 100 for CIFAR-100.

Baseline attack setting. Inspired by the works from [5, 10], we design the baseline attack in FL for the target-on-demand and imperceptible settings to compare with our method. This baseline setting of the multi-target and imperceptible attack is called BadNets-MT. Considering the CIFAR-10 task, we create 10 fixed patterns of shapes 0, 1, 2, 3, 4, 5, 6, 7, 8, 9. Whenever a pattern with the number i is patched onto an image, the global model will predict that image as the target class i ($i \in \{0, 1, 2, \dots, 9\}$). By default, each fixed trigger is added on the top left corner of the image. We use the following function to generate the image x from the original dataset \mathcal{D} with a fixed trigger Δ and a blend ratio $\gamma \in [0, 1]$:

$$x_{poison} = (1 - \gamma) \cdot x + \gamma \cdot \Delta \cdot mask$$

Here, all elements of $mask$ are 0s except for the positions where the trigger is patched. Those positions are 1s. The purpose of the blend ratio γ is to control the visibility of the trigger so that the poisoned image is imperceptible to human beings. Inspired by [5], we choose $\gamma = 0.001$ in training to insert a stealthy trigger

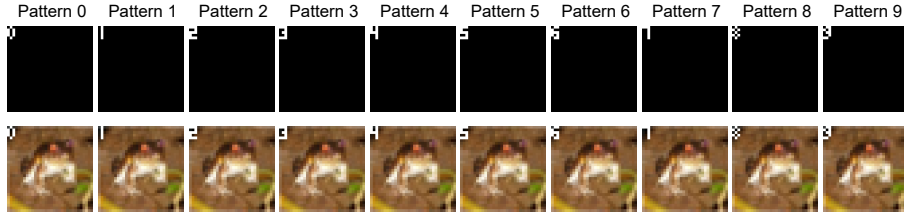


Fig. 9: The 10 fixed patterns serve as 10 triggers so that when one image is patched onto the top left corner of the image, the global model will predict that image as the trigger-like target class

to generate poisoned data and do not use the blend ratio during inference to take advantage of the easy-implementability in practice as in the Accessory Injection strategy [5]. The function used to generate poisoned images without the blend ratio is:

$$x_{poison} = x + \Delta \cdot mask$$

The visualization of the patterns is shown in Figure 9.

Setting for the ϵ -bounded approach. Follow prior works [7, 22] on using a small upper bound $\epsilon > 0$ on the adversarial noise in order to make the noise small enough so that the images patched with the noise are similar to the original ones, we design experiments to compare with Venomancer by using the formulas below to create poisoned images:

$$\delta = \mathcal{G}_{\xi}(x, y_{target}) \cdot \epsilon; x_{poison} = \text{Clip}(x + \delta)$$

A.3 Hyperparameters for our proposed attack

Controlling coefficient for training generator β . When training a generator at stage 1, the generator is trained to achieve two tasks: (1) to generate poisoned images that are imperceptible to human beings and (2) to make the global model predict poisoned images as the arbitrarily attacker-chosen class. The first task is achieved by minimizing the visual loss \mathcal{L}_{visual} , *i.e.* the cosine distance function, between the original image and the poisoned image. The second task is achieved by minimizing the backdoor loss $\mathcal{L}_{backdoor}$, *i.e.* the cross-entropy loss between the global model’s prediction and the target class. Coefficient β is used to control the strength of the loss signals from the two tasks. In our experiments, we choose $\beta = 0.01$ for MNIST, F-MNIST, and CIFAR-10, and $\beta = 0.004$ for CIFAR-100.

Controlling coefficient for injecting backdoor α . In our studies, the α controls the strength of the clean loss \mathcal{L}_{clean} and the backdoor loss $\mathcal{L}_{backdoor}$, *i.e.* the cross-entropy loss, during the local training. If α is large, *i.e.* $\alpha > 0.5$,

the classifier’s performance on clean data will be quickly converged to the optimum. When α is small, *i.e.* $\alpha < 0.5$, the classifier’s performance on backdoor or poisoned data will rapidly achieve a high value. If the generator \mathcal{G} is properly trained, *i.e.* the learning speed of \mathcal{G} is the same as the learning speed of the classifier, the poisoned classifier still converges to the same optimal performance on both clean and backdoor tasks. So we select $\alpha = 0.5$ for all tasks.

The learning rate atk_lr of the generator \mathcal{G} . This parameter controls the learning speed of the generator \mathcal{G} during the local training of a malicious client. Empirically, the learning rate atk_lr is suggested to be in the range (0.0001, 0.001). In our experiments, we choose $atk_lr = 0.0002$ for all tasks.

The number of poisoning epochs E_{poison} . In our framework, the trigger generator and the classifier are trained in an alternating manner. First, the generator is trained for E_{poison} epochs, then the classifier is trained for E epochs. Increasing E_{poison} can help the attack to be more effective. However, it also increases the computational cost. In our work, we choose $E_{poison} = 5$ for all tasks.

The number of malicious clients. The number of malicious clients is a crucial factor that affects the backdoor accuracy and imperceptibility of the attack. In our experiments, we choose the number of malicious clients to be 2% of the total clients, *i.e.* 2 clients, for all tasks.

A.4 Hyperparameters for the selected defenses

In this paper, we select four state-of-the-art defenses, *i.e.* Norm Clipping [28], Weak DP [28], Krum [4], and Multi-Krum [4] to evaluate the effectiveness of our method. By default, the hyperparameters for the defenses are set up as in the original papers.

Norm Clipping. Norm Clipping clips the updates from clients when they exceed a certain threshold. This defense effectively constrains the behavior of clients to prevent the global model from being overwhelmed by a small number of clients. The threshold is set to 1 by default.

Weak DP. Weak DP introduces Gaussian noise $z \sim \mathcal{N}(0, \sigma^2)$ to clients’ updates to perturb carefully crafted malicious updates. It should be noted that this mechanism is not tailored for privacy preservation, hence the Gaussian noise is of a smaller magnitude compared to that used in strict differential privacy practices. The standard deviation σ is set to 0.002 by default.

Krum/Multi-Krum. Krum chooses a client or clients whose updates are closest in terms of L2 distance to the updates of other clients. These selected clients are then used to update the global model. While this method is effective at enhancing the model’s robustness by excluding many updates, it can also have an impact on the model’s accuracy. Multi-Krum is an extension of Krum that selects multiple such clients to update the global model.

B Additional Experiments for our method

B.1 Comparison with the baseline attack BadNets-MT

We compare our method with various blend ratios γ of the baseline attack BadNets-MT on CIFAR-10. In this experiment, we extend the FL training to 900 rounds and choose γ values for imperceptible triggers. In terms of the Clean Accuracy (CA), Venomancer achieves a CA of around 70%, which is comparable with the line $\gamma = 0.001$. There are fluctuations in the CA with different γ values. In Figure 10, we show that only $\gamma = 0.001$, $\gamma = 0.015$, and $\gamma = 0.02$ reach more than 60% at the end of the FL training, while the lines for the other γ never reaches 60% during the entire training period. Regarding the Backdoor Accuracy (BA), Venomancer outperforms BadNets-MT for various values of γ . The BA of Venomancer increases quickly to more than 90% for the first 200 rounds and remains stable at around 98% for the rest of the training. In contrast, the BA of BadNets-MT remains at around 10% during the first 200 rounds. After that, we observe an increase in the BA to around 55% and 57% for $\gamma = 0.015$ and $\gamma = 0.02$ then the BAs decrease to about 40% and 37% onwards, respectively. The phenomenon of remaining at a low BA for a while and then increasing to a higher BA is also observed in $\gamma = 0.01$ and $\gamma = 0.005$. For the one that is comparable with Venomancer’s CA, $\gamma = 0.001$, its BA remains at below 10% during the whole training. The visualization is shown in Figure 10.

B.2 Assessing the imperceptibility of diverse poisoned images

We visualize the clean and backdoor images for MNIST, F-MNIST, and CIFAR-10 in Figure 11. Our experiments show that the poisoned global model makes a decision for the backdoor image based on the same region as the clean image. Moreover, the backdoor images are impressively visible to human beings, thus emphasizing the stealthiness of our attack.

B.3 Backdoor accuracy for each attacker-chosen target class

Since our method aims to make the poisoned global model misclassify an input patched with a trigger as any attacker-chosen target class without dropping much in the CA, we evaluate the BA of each target class for Venomancer. The results in Table 5 show the effectiveness of our attack when it achieves 100% BA for almost all target classes on MNIST, F-MNIST, and CIFAR-10. Note that for F-MNIST, 0: T-shirt, 1: Trouser, 2: Pullover, 3: Dress, 4: Coat, 5: Sandal, 6: Shirt,

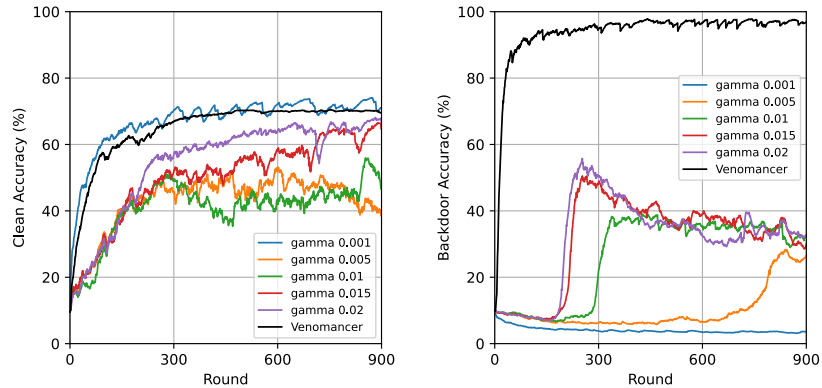


Fig. 10: The effectiveness of Venomancer is compared with the baseline attack BadNets-MT for different blend ratios γ on CIFAR-10. Our method shows a much higher BA than the baseline with the same imperceptibility.

Table 5: The BA (%) of each target class of our method for MNIST, F-MNIST, and CIFAR-10 tasks

Dataset	Attacker-chosen target class									
	0	1	2	3	4	5	6	7	8	9
MNIST	100	100	100	100	100	100	100	100	100	100
F-MNIST	100	99.90	100	100	100	89.13	100	100	100	98.30
CIFAR-10	100	100	100	100	100	100	100	100	100	100

7: Sneaker, 8: Bag, 9: Ankle boot. For CIFAR-10, 0: Airplane, 1: Automobile, 2: Bird, 3: Cat, 4: Deer, 5: Dog, 6: Frog, 7: Horse, 8: Ship, 9: Truck.

B.4 Attack effectiveness under different models

Different classification models. We evaluate the transferability of the generator to different classification models. In our experiments, we compare VGG11 [27] and ResNet-18. For MNIST, F-MNIST, and CIFAR-10, we train the models from scratch. For CIFAR-100, we use a pre-trained VGG11 and a pre-trained ResNet-18, both of which are trained for 60 epochs. Our results are shown in Table 6.

Different generator models. In this section, we evaluate the effectiveness of our method under different generator models, *i.e.* Conditional Autoencoder and Conditional U-Net. Our results in Table 7 show that there are not many differences in the BA and CA between the chosen architectures.

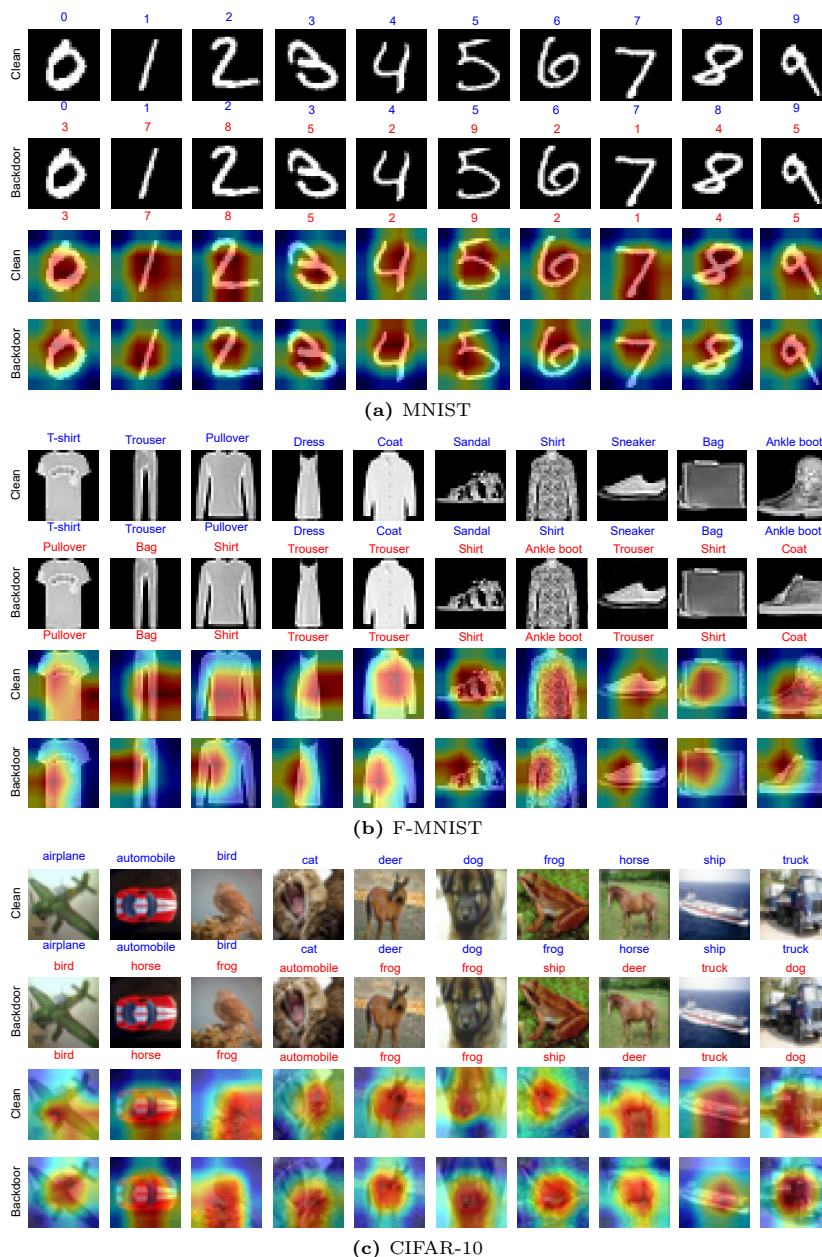


Fig. 11: The view of clean and backdoor images for MNIST, F-MNIST, and CIFAR-10 on the first two rows, and Grad-CAM [26] visualizations of clean and backdoor images on the last two rows, respectively. Blue and red on top of each image mean the true label and the target class in order. Blue and red under each image mean the predicted label for clean and backdoor images, respectively.

Table 6: Our method remains effective for both VGG11 and ResNet-18 architectures

Classifier	MNIST		F-MNIST		CIFAR-10		CIFAR-100	
	CA (%)	BA (%)	CA (%)	BA (%)	CA (%)	BA (%)	CA (%)	BA (%)
VGG11	99.27	99.59	90.74	86.55	69.65	99.87	43.70	99.15
ResNet-18	99.51	100	92.14	96.62	71.3	99.83	60.94	99.75

B.5 Attack effectiveness under various heterogeneous degrees

We explore the effectiveness of Venomancer under different φ values in the Dirichlet distribution on the four chosen datasets, *i.e.* MNIST, F-MNIST, CIFAR-10, and CIFAR-100. This highlights the stability and resilience of our method when deployed in conventional FL settings. Table 8 presents the results of CA and BA under different φ values in the Dirichlet distribution.

B.6 Attack effectiveness under different attack frequencies

We evaluate our attack’s effectiveness under different attack frequencies, *i.e.* $f \in \{1, 2, 5, 10\}$. The results in Table 9 show that the BA of Venomancer remains high across all datasets, even when the attack frequency is increased.

B.7 Attack effectiveness under various numbers of malicious clients

We test our attack with different numbers of malicious clients $P \in \{1, 2, 5\}$. Our results in Table 10 show that the BA of Venomancer remains effective across all datasets.

C Societal Impact

Our research aims to enhance recognition and comprehension of vulnerabilities encountered during the training of neural networks in FL settings. If misapplied or in the absence of more robust defenses, the attack we have introduced could pose risks to current FL applications. We view our contributions as crucial for grasping the extent of backdoor attacks within FL settings. We expect that these insights will encourage the advancement of more secure FL frameworks and the creation of stronger defenses.

Table 7: Our method remains effective for both Conditional Autoencoder and Conditional U-Net architectures

Generator	MNIST		F-MNIST		CIFAR-10		CIFAR-100	
	CA (%)	BA (%)	CA (%)	BA (%)	CA (%)	BA (%)	CA (%)	BA (%)
Conditional U-Net	99.53	100	92.63	99.52	74.2	100	60.94	99.75
Conditional Autoencoder	99.51	100	92.14	96.62	71.3	99.83	60.70	92.20

Table 8: The CA and BA of Venomancer under different φ values in the Dirichlet distribution

Task	$\varphi = 0.2$		$\varphi = 0.5$		$\varphi = 0.7$		$\varphi = 0.9$	
	CA (%)	BA (%)	CA (%)	BA (%)	CA (%)	BA (%)	CA (%)	BA (%)
MNIST	99.57	100	99.51	100	99.60	100	99.52	99.99
F-MNIST	92.15	98.44	92.14	96.62	92.71	92.65	92.67	92.68
CIFAR-10	72.66	99.16	71.3	99.83	73.87	99.83	73.61	99.97
CIFAR-100	61.09	99.15	60.94	99.75	60.82	99.74	61.17	99.66

Table 9: The CA and BA of Venomancer under different attack frequencies f

Task	$f = 1$		$f = 2$		$f = 5$		$f = 10$	
	CA (%)	BA (%)	CA (%)	BA (%)	CA (%)	BA (%)	CA (%)	BA (%)
MNIST	99.51	100	99.54	96.61	99.55	93.00	99.60	95.45
F-MNIST	92.14	96.62	92.41	91.84	92.60	90.70	92.70	90.97
CIFAR-10	71.30	99.83	74.36	100	74.01	95.81	73.76	96.50
CIFAR-100	60.94	99.75	61.97	99.57	62.09	98.85	62.09	98.46

Table 10: The CA and BA of Venomancer under different numbers of malicious clients

Task	$P = 1$		$P = 2$		$P = 5$	
	CA (%)	BA (%)	CA (%)	BA (%)	CA (%)	BA (%)
MNIST	99.53	91.87	99.51	100	99.61	100
F-MNIST	92.72	83.42	92.14	96.62	91.96	99.92
CIFAR-10	75.68	95.05	71.30	99.83	69.95	100
CIFAR-100	61.80	99.23	60.94	99.75	57.81	99.96